Optical Transfer Function Measurements for Technically Premixed Flames

Bruno Schuermans
Felix Guethe
Wolfgang Mohr

Alstom,
Baden CH-5405,
Switzerland

This paper deals with a novel approach for measuring thermoacoustic transfer functions. These transfer functions are essential to predict the acoustic behavior of gas turbine combustion systems. Thermoacoustic prediction has become an essential step in the development process of low NO_x combustion systems. The proposed method is particularly useful in harsh environments. It makes use of simultaneous measurement of the chemiluminescence of different species in order to obtain the heat release fluctuations via inverse method. Generally, the heat release fluctuation has two contributions: one due to equivalence ratio fluctuations, and the other due to modulations of mass flow of mixture entering the reaction zone. Because the chemiluminescence of one single species depends differently on the two contributions, it is not possible to quantitatively estimate the heat based on this information. Measurement of the transfer matrix based on a purely acoustic method provides quantitative results, independent of the nature of the interaction mechanism. However, this method is difficult to apply in industrial full-scale experiments. The method developed in this work uses the chemiluminescence time traces of several species. After calibration, an overdetermined inverse method is used to calculate the two heat release contributions from the time traces. The optical method proposed here has the advantage that it does not only provide quantitative heat release fluctuations but it also quantifies the underlying physical mechanisms that cause the heat release fluctuations: It shows what part of the heat release is caused by equivalence ratio fluctuations and what part by flame front dynamics. The method was tested on a full scale swirl-stabilized gas turbine burner. Comparison with a purely acoustic method validated the concept.
[DOI: 10.1115/1.3124663]

1 Introduction

Modern design of low emission combustors is characterized by swirling air in the combustor's dome coupled with distributed fuel injection to maximize mixing. This design results in efficient combustion with extremely low emissions.

Because of a complex interaction between several physical processes, the thermoacoustic dynamics of a swirl-stabilized flame can be very difficult to model accurately. Experimentally obtained transfer matrices are crucial to validate acoustic flame models. Besides validation, the measured transfer functions can give more physical insight to the interactions occurring in the flame. A measured transfer function may also be used directly in an acoustic network, treating the flame element as a "black box."

The idea of experimentally determining the coefficients of an acoustic system represented as a black box with two inputs, two outputs, and two source terms date back to the 1970s [1]. Bodén et al. [2] applied this technique extensively to several cold flow applications. The idea of using this method to obtain acoustic transfer matrices of combustion processes originates from Paschereit and Polifke [3,4]. The method was further developed and validated [5–7] and is now a well established tool that proves to be the key experimental method in thermoacoustic analysis at Alstom. The measured transfer matrices were successfully used to predict stability and pulsation spectra of Alstom gas turbines [8].

The rather harsh conditions in full scale, full pressure test facilities make highly accurate acoustic measurements difficult. This motivated the development of an optical technique for measuring flame transfer functions. Optical flame transfer function measurements are not a novelty at all. This technique was extensively used by many researchers [9,10]. Generally, the chemiluminesence signal is assumed to be proportional to the heat release. This method is valid and straightforward for perfectly premixed flames. However, as pointed out by Schuermans et al.[7], Auer et al. [11], and Haber et al. [12], such an approach yields erroneous results if applied to flames where fluctuations of equivalence ratio are present. The reason why the method does not work in these cases is that the chemiluminesence signal reacts stronger on an equivalence ratio fluctuation than on a mass flux modulation. Thus, if a certain intensity fluctuation is measured, it is impossible to know how large the corresponding heat release fluctuation is. Higgins and co-workers [13,14] did systematic measurements on OH^* and CH^* chemiluminesence intensity of methane flames and found that the chemiluminesence intensity reacts stronger to fuel concentration variation than to mixture mass flux variation. This is a serious limitation of this technique for application to lean premixed gas turbine burners because all these burners are technically premixed and hence equivalence ratio fluctuations can never be excluded.

Chemiluminesence has typically a power law or exponential dependence on temperature (or equivalence ratio) and a proportional dependence on mass flux. The different radicals in the flame have typically a different exponential factor. This property was exploited by Higgins et al. [14] and later by Hardalupas and Orain [15] by taking the ratio of two chemiluminesence signals as an indicator of (steady) equivalence ratio. A different but conceptually similar approach is used by Ayoola et.al [16] where information of simultaneous laser induced fluorescence (LIF) images of different species is combined to visualize heat release.

In this paper, the idea was extended to measure flame transfer matrices of flames where equivalence ratio fluctuations may be present. The idea is to measure at least two chemiluminesence

Contributed by the International Gas Turbine Institute of ASME for publication in the JOURNAL OF ENGINEERING FOR GAS TURBINES AND POWER. Manuscript received April 1, 2008; final manuscript received April 11, 2008; published online May 6, 2010. Review conducted by Dilip R. Ballal. Paper presented at the ASME Turbo Expo 2008: Land, Sea, and Air (GT2008), Berlin, Germany, June 9–13, 2008.

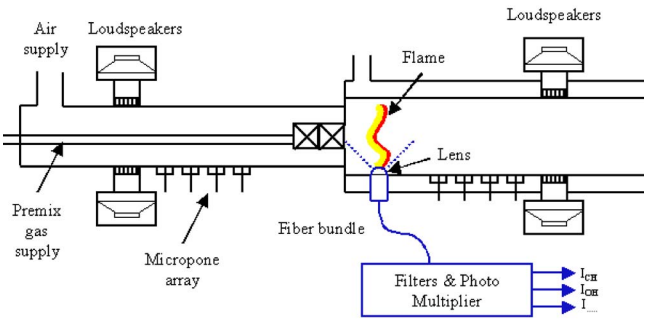

Fig. 1 Experimental setup: atmospheric pressure combustion test equipped facility with loudspeakers, microphones, and optical access via a fiber bundle

intensity signals. In the first step, steady state calibration curves are measured. These calibration curves are linearized and inverted to convert measured fluctuating intensity signals into signals representing mixture mass flux and fuel mass fraction fluctuations. The heat release fluctuation is then obtained as the sum of these two fluctuations. In this way not only a quantitative estimate of the heat release fluctuation is obtained but the method also shows by what mechanisms the heat released fluctuation are caused.

A proof of concept is delivered by testing this method on a prototype gas turbine burner and by comparing the results with a purely acoustic method to measure the heat release fluctuations.

2 Experimental Setup

2.1 Atmospheric Combustion Facility. The tests were performed in an atmospheric pressure, single burner combustion test facility with a full-scale prototype gas turbine burner. The test rig is shown in Fig. 1. The test rig consists of a plenum chamber upstream of a swirl-inducing burner and a combustion chamber downstream of the burner. The circular combustion chamber consists of an air cooled double walled metal liner. Combustion air is electrically preheated, fed into a plenum chamber, and flows from there through the burner and the combustion chamber. The exhaust system is an air-cooled tube with the same cross section as the combustion chamber to avoid acoustic reflections at area discontinuities. The acoustic boundary conditions of the exhaust system can be adjusted from almost anechoic (reflection coefficient $|r|<0.15$) to open end reflection by means of suitably dimensioned orifice plates.

The test was performed on an Alstom EV-type test burner. Such a burner has the unique property of flame stabilization in free space near the burner outlet utilizing the sudden breakdown of a swirling flow, called vortex breakdown. The swirler consists of two halves of a cone, which are shifted to form two air slots of constant width [17]. Gaseous fuels are injected into the combustion air by means of fuel distribution tubes comprising two rows of small holes perpendicular to the inlet ports of the swirler. Complete mixing of fuel and air is obtained shortly after injection.

2.2 Acoustic Measurement Setup. Pressure fluctuations are measured using Brüel and Kjær water-cooled microphones. The water-cooled $\frac{1}{4}$ in. condenser microphones are flush mounted on the walls of the plenum chamber and combustion chamber. The holder consists of a small orifice ($d=0.5$ mm) open to the combustion chamber. The microphone diaphragm is placed in a small cavity and is protected from heat radiation. The resonance frequency f_{res} of the holder is larger than 20 kHz. Using condenser microphones rather than piezoelectric pressure transducers has the advantage of highly accurate phase and amplitude data, which is necessary for acoustic measurements. The frequency response of the microphones in probe holders were compared against standard B&K microphones and showed good agreement. A total of nine axially distributed microphones were used: four in the plenum chamber and five in the combustion chamber. Controlled excitation of the acoustic field was accomplished by a circumferential array of four loudspeakers equally spaced in polar angles. One set of loudspeakers was placed in the plenum chamber at a distance $x/D=4.2$ upstream of the dump plane and the second at $x/D=6.8$ downstream of the dump plane, where D is the diameter of the combustion chamber.

2.3 Optical Setup. The light emitted by the flame is collected through a water-cooled window by a lens system. The optical detection was accomplished by a nonimaging system of quartz lenses focusing the light on seven different fibers. This setup assures that each fiber obtains the same light and avoids angle dependency. The lens was optimized in order to minimize the intensity dependence from flame position. This is important in order to avoid that the flame movement is interpreted as intensity fluctuation. The opening angle of the system was chosen such that the entire heat release zone was covered. The geometrical extent and movement of the heat release zone are known from previous flame visualization studies.

The light is then distributed to a system of filters and detectors. This yields five separate signals for five different wavelength regions. These chemiluminesence signals are recorded simultaneously with the microphone signals on the same data acquisition system. The optical setup was tested on a Bunsen flame with five different band pass filters of about 10 nm width at central widths (CWs) of 307 nm, 431 nm, 450 nm, and 515 nm, and one UV transparent broad band filter (DUGX11, Schott). The transmission curves are shown in Fig. 2. Using this optical setup, the different channels can be attributed to the occurrence of chemiluminescence of mainly the species (OH^*, CH^*, C_2^*), as indicated in Refs. [15,18]. To monitor the broad emission (attributed to the $CO+O \rightarrow CO_2^*$ chemiluminescence), which contributes as background in the spectrum [19], a filter with CW of 450 nm is used. All channels mainly detect emission from different species probing a different part of the flame chemistry. Each of these detection windows scales differently with the operating parameters mass flow and flame temperature. With the calibration of at least three averaged steady operating points, this ratio of the channels allows the interpretation as instantaneous measurements of these operating parameters. This reading can be interpreted as fluctuations of the governing heat release parameters (adiabatic flame temperature and mixture mass flow), as described in Refs. [13,14]. A further correlation of the signals to individual molecular emissions utilizing the spectra can be undertaken and would improve the quality of the interpretation. However, because it is not necessary for the approach described in this work, this was omitted here.

3 Analysis of Optical Data

The heat release rate does not only depend on equivalence ratio but is given (for a combustion efficiency of 100%) by the following expression:

$$Q = m_f H_f = m y H_f \tag{1}$$

where m_f and m are the instantaneous values of the mass fluxes of fuel and mixture entering the reaction zone, y is the mass fraction of fuel ($y=m_f/m$), and the chemical enthalpy of the fuel is represented as H_{fuel}.

The mass flux of the mixture through the flame front fulfills the following equality: $m_f+m_a=\int \rho S dA=\rho S_{\text{flame}} A_{\text{flame}}$. The definition of the flame surface and flame velocity is somewhat arbitrary. However, the definition of both quantities should be such that the product of flame speed and flame area conserves mass across the flame front. Please note that in the following, all relevant quantities are considered as averages of the quantity over the flame surface (hence assuming homogeneity of the time-averaged quantities and linearity of the perturbations).

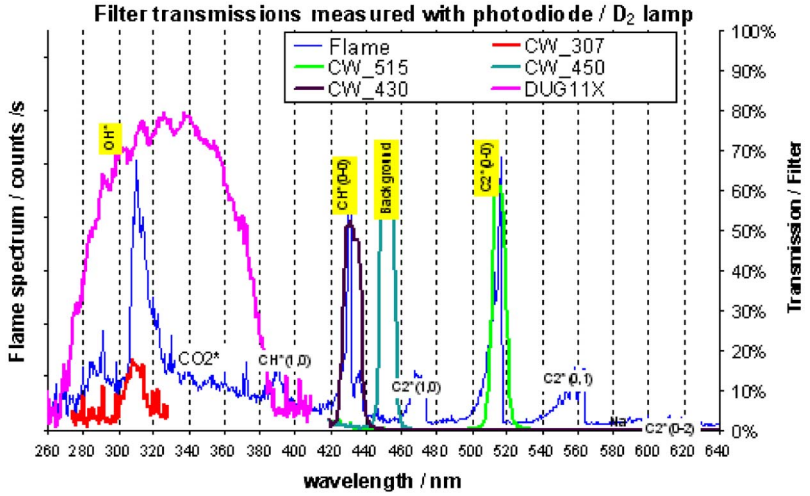

Fig. 2 Transmission curve of the filters used and flame spectrum from a test flame

Experimental studies by several authors have shown that the dependence of OH chemiluminescence on mass flux and equivalence ratio is not the same. For example, Higgins et al. [13] reported the following experimental correlation for the OH^* chemiluminescence:

$$I = km\phi^{\alpha}p^{\beta} \tag{2}$$

with $\alpha=5.23$ and $\beta=-0.86$. It should be noted that the experiments were performed in a range of operating conditions that did not cover the range of our experiments (a higher mixture temperature was used in our experiments). Nevertheless, the correlation suggests that care should be taken when interpreting chemiluminescence intensity as a measure for the heat release of technically premixed flames. For example, if an intensity amplitude of 10% of the mean is measured, then this could be due to a 10% fluctuation of mass flow or due to 10/5.23% fluctuation of equivalence ratio (which would be associated with a 5.23 times smaller heat release fluctuation). Thus, if it is not known in advance what the cause of the intensity fluctuation is, then an error of 500% is introduced.

The present work deals with acoustic phenomena. That is why only small perturbation of the flow conditions are considered, which justifies a linearization of Eqs. (1) and (2):

$$\frac{Q'}{\bar{Q}} = \frac{m'}{\bar{m}} + \frac{y'}{\bar{y}} \tag{3}$$

in which a prime denotes a perturbation and an overbar signifies the mean quantity: $x(t)=\bar{x}+x'(t)$.

Similarly, the linearization of Eq. (2) yields

$$\frac{I'}{\bar{I}} = \frac{m'}{\bar{m}} + \alpha\frac{y'}{\bar{y}} + \beta\frac{p'}{\bar{p}} \tag{4}$$

Note that

$$\frac{m'}{\bar{m}} = \frac{S_f'}{\bar{S}_f} + \frac{A_f'}{\bar{A}_f} + \frac{\rho'}{\bar{\rho}} \tag{5}$$

Thus, the mass flow fluctuations of the mixture entering the reaction zone can also be interpreted as flame area fluctuations and/or flame velocity fluctuations.

Because $m'/\bar{m}$ is expected to be of order $u'/\bar{u}$, it can be shown that the influence of density fluctuations can be neglected for low Mach number flow.

$$\frac{\rho'}{\bar{\rho}} = \frac{p'}{\gamma\bar{p}} \approx \frac{\bar{\rho}cu'}{\gamma\bar{p}} = \frac{u'}{c} \ll \frac{u'}{\bar{u}} \approx \frac{m'}{\bar{m}} \tag{6}$$

The use was made of $u' \approx p'/(\bar{\rho}c)$, which is justified because the spatial maximum amplitude of oscillation of pressure is related to the maximum amplitude of velocity by $|\hat{u}|_{\max}=|\hat{p}|'_{\max}/(\bar{\rho}c)$. For the Mach number range of our experiment, the relative pressure fluctuations are one to two orders of magnitude smaller than the relative velocity fluctuations. That is why the influence of pressure or density fluctuations in Eqs. (4) and (5) will be neglected.

Comparing Eqs. (3) and (4), it can be concluded that in the absence of equivalence ratio fluctuations ($y'=0$), the relative heat release fluctuations are equal to the relative intensity fluctuations.

$$\frac{Q'}{\bar{Q}} = \frac{I'}{\bar{I}} \tag{7}$$

In absence of mass flux fluctuations ($m'=0$), the heat release fluctuations are related to intensity fluctuations as

$$\frac{Q'}{\bar{Q}} = \frac{I'}{\alpha\bar{I}} = \frac{I'}{\frac{\partial I}{\partial y}} \tag{8}$$

Thus, if the chemiluminescence intensity is used as a measure for heat release, one should have prior knowledge of the underlying physical mechanism causing the heat release fluctuations. Both contributions of y' and m' can be expected in technically premixed burners (i.e., when mixing of air and fuel takes place in the burner). In most cases of practical relevance, it is impossible to exclude any of the two contributions a priori.

So, for cases where both $m'/\bar{m}$ and $y'/\bar{y}$ could be important, the chemiluminesence signal is not a measure for heat release (provided α is not equal to 1). Typical values for α range between 5 and 10; thus the error introduced by a wrongly assumed physical mechanism is of the order of 1000%.

In this work a method is presented that overcomes this problem. The method uses chemiluminescence of at least two species as input and calculates the heat release from these signals via an inverse operation. Thus, measurement of the intensity of two species would result in two relations like in Eq. (4). Denoting the two species by subscripts 1 and 2, these two equations can be written in matrix form as

$$\begin{bmatrix} \frac{I_1'}{\bar{I}_1} \\ \frac{I_2'}{\bar{I}_2} \end{bmatrix} = \begin{bmatrix} 1 & \alpha_1 \\ 1 & \alpha_2 \end{bmatrix} \begin{bmatrix} \frac{m'}{\bar{m}} \\ \frac{y'}{\bar{y}} \end{bmatrix} \tag{9}$$

If $\alpha_1 \neq \alpha_2$, then the system can be inverted in order to calculate $m'/\bar{m}$ and $y'/\bar{y}$ from measured $I_1'/\bar{I}_1$ and $I_2'/\bar{I}_2$.

This concept can be extended to the more general case with K species and a model structure different from Eq. (2) by linearization of the intensity functions.

$$\begin{bmatrix} \frac{I_1'}{\bar{I}_1} \\ \vdots \\ \frac{I_K'}{\bar{I}_K} \end{bmatrix} = \begin{bmatrix} \frac{\bar{m}}{I_1}\frac{\partial I_1}{\partial m} & \frac{\bar{y}}{I_1}\frac{\partial I_1}{\partial y} \\ \vdots & \vdots \\ \frac{\bar{m}}{I_K}\frac{\partial I_K}{\partial m} & \frac{\bar{y}}{I_K}\frac{\partial I_K}{\partial y} \end{bmatrix} \begin{bmatrix} \frac{m'}{\bar{m}} \\ \frac{y'}{\bar{y}} \end{bmatrix} = \mathbf{J} \begin{bmatrix} \frac{m'}{\bar{m}} \\ \frac{y'}{\bar{y}} \end{bmatrix} \tag{10}$$

The matrix $\mathbf{J}$ is thus a normalized Jacobian matrix of the intensity functions. In the case of $K>2$, the system is overdetermined and hence the system has to be inverted in least-squares sense:

$$\begin{bmatrix} \frac{m'}{\bar{m}} \\ \frac{y'}{\bar{y}} \end{bmatrix} = \mathbf{J}^{\dagger} \begin{bmatrix} \frac{I_1'}{\bar{I}_1} \\ \vdots \\ \frac{I_K'}{\bar{I}_K} \end{bmatrix} \tag{11}$$

in which the following notation was introduced: $X^{\dagger} \equiv (X^* X)^{-1} X^*$, where the asterisk denotes the transposed complex conjugate of the matrix.

This equation can either be applied to the time traces of the signals $I'(t)$ or to the Fourier coefficient of the transformed signal $\hat{I}(\omega)$. In order to apply this method, the derivatives of the intensities with respect to the mass flow and fuel fraction need to be known. These can be obtained from a set of calibration measurements where the chemiluminescence intensities of all the species are measured while changing the time-averaged mass flow and fuel fraction. The derivatives can be obtained by approximating them by finite differences of the data. However, in this work a curve fit with equations similar to Eq. (1) is performed, and the derivatives of these curves are obtained analytically.

With heat release fluctuations measured in this way, a flame transfer function can be obtained if the acoustic velocity fluctuation in front of the flame is measured. In the case of a negligible effect of the influence of pressure on the heat release fluctuation, the transfer function is obtained as

$$F(\omega) = \frac{\hat{Q}}{\hat{u}_1}\frac{\bar{u}_1}{\bar{Q}} \tag{12}$$

Note that generally $\hat{u}_1/\bar{u}_1 \neq \hat{m}/\bar{m}$, this is because m is defined as the instantaneous mass flux of mixture taking part in reaction, which is equal to the integral of the product of flame area, flame speed, and density over the flame area. In the steady state, both quantities will be equal (up to order of M^2), but for higher frequencies, the flame front dynamics (i.e., the kinematic response of the instantaneous flame front location and area to a velocity perturbation) will cause a frequency dependent difference between the two.

The optical method proposed here has the advantage since it does not only provide quantitative heat release fluctuations but it also quantifies the underlying physical mechanisms that cause the heat release fluctuations: It shows what part of the heat release is caused by equivalence ratio fluctuations and what part by flame front dynamics. To exploit this even more, the dependence of the fluctuations of mass flux and mass fraction on the acoustic pressure and velocity is investigated. These quantities are related by a transfer matrix C:

$$\begin{bmatrix} \frac{\hat{m}}{\bar{m}} \\ \frac{\hat{y}}{\bar{y}} \end{bmatrix} = \begin{bmatrix} C_{11} & C_{12} \\ C_{21} & C_{22} \end{bmatrix} \begin{bmatrix} \frac{\hat{p}_1}{\bar{u}_1} \\ \frac{\hat{u}_1}{\bar{u}_1} \end{bmatrix} \tag{13}$$

Note that the matrix is a function of frequency and that the Fourier coefficients of the pressure are normalized by ρc, thus $\hat{p}(\omega)$ has units of m/s. In order to obtain the four matrix elements from the experimental data, at least two linearly independent test states are required. These test states are generated by consecutively applying forcing with the upstream and downstream loudspeakers. Denoting the upstream forcing test results with superscript A and the downstream excitation case with superscript B, the matrix C is obtained as

$$\begin{bmatrix} C_{11} & C_{12} \\ C_{21} & C_{22} \end{bmatrix} = \begin{bmatrix} \frac{\hat{m}^A}{\bar{m}} & \frac{\hat{m}^B}{\bar{m}} \\ \frac{\hat{y}^A}{\bar{y}} & \frac{\hat{y}^B}{\bar{y}} \end{bmatrix} \begin{bmatrix} \hat{p}_1^A & \hat{p}_1^B \\ \hat{u}_1^A & \hat{u}_1^B \end{bmatrix}^{-1} \frac{1}{\bar{u}_1} \tag{14}$$

The pressure and velocity fluctuations $\hat{u}_1$ and $\hat{p}_1$ can be obtained from acoustical measurements. This is done using the microphones placed before and after the burner together with the multimicrophone method as will be explained in Sec. 4.

The Rankine–Hugoniot relations give the following relations between the acoustic velocities on both sides of a low Mach number interface with heat release:

$$\hat{u}_2 = \hat{u}_1 + \left(\frac{T_2}{T_1} - 1\right)\bar{u}_1 \frac{\hat{Q}}{\bar{Q}} \tag{15}$$

From the definition of the flame transfer matrix and Eqs. (13) and (15), it follows that the transfer matrix elements are given by

$$F_{21} = \left(\frac{T_2}{T_1} - 1\right)(C_{11} + C_{21}) \tag{16}$$

$$F_{22} = 1 + \left(\frac{T_2}{T_1} - 1\right)(C_{12} + C_{22}) \tag{17}$$

4 Transfer Matrix Measurement

The acoustic transfer matrix T of an acoustic system gives the dynamic relation between the acoustic fields on both sides of the system. It is defined here as

$$\begin{bmatrix} \hat{p}_d \\ \hat{u}_d \end{bmatrix} = \begin{bmatrix} T_{11} & T_{12} \\ T_{21} & T_{22} \end{bmatrix} \begin{bmatrix} \hat{p}_u \\ \hat{u}_u \end{bmatrix} \tag{18}$$

The subscripts d and u refer to locations upstream and downstream of the element. The symbols $\hat{p}$ and $\hat{u}$ represent acoustic pressure and velocity. These quantities correspond to the unsteady irrotational part of the pressure and velocity field.

The four frequency dependent elements of the transfer matrix T are obtained by forcing the system with loudspeakers and measuring the response with microphones. A detailed description of this technique is given in Ref. [7]. The most important aspects will be repeated here. Because Eq. (18) provides two equations in four unknowns, at least two independent test states are required to extract the four elements of T. Thus, using the same notation as in Eq. (14), the transfer matrix is obtained as

$$\begin{bmatrix} T_{11} & T_{12} \\ T_{21} & T_{22} \end{bmatrix} = \begin{bmatrix} \hat{p}_d^A & \hat{p}_d^B \\ \hat{u}_d^A & \hat{u}_d^B \end{bmatrix} \begin{bmatrix} \hat{p}_u^A & \hat{p}_u^B \\ \hat{u}_u^A & \hat{u}_u^B \end{bmatrix}^{-1} \tag{19}$$

The multimicrophone method is used in order to obtain the acoustic velocity and pressure at the reference position from data of acoustic pressure at multiple microphone locations. It makes use of the solution of the one dimensional wave equation in presence of mean flow $\hat{p}(\omega,x)=\hat{f}(\omega)e^{-i(\omega/c)(x/(1+M))}+\hat{g}(\omega)e^{i(\omega/c)(x/1-M)}$, in which the Riemann invariants $\hat{f}(\omega)$ and $\hat{g}(\omega)$ are integration constants whose values depend on the initial conditions and boundary conditions. The acoustic pressure measured by N microphones in a straight duct at positions x_n can thus be expressed as

$$\begin{bmatrix} \hat{p}_1 \\ \vdots \\ \hat{p}_N \end{bmatrix} = \begin{bmatrix} z_1^{(1/1+M)} & z_1^{(-1/1-M)} \\ \vdots & \vdots \\ z_N^{(1/1+M)} & z_N^{(-1/1-M)} \end{bmatrix} \begin{bmatrix} \hat{f} \\ \hat{g} \end{bmatrix} = Z \begin{bmatrix} \hat{f} \\ \hat{g} \end{bmatrix} \tag{20}$$

in which the following notation $z_n \equiv e^{-i(\omega x_n/c)}$ is used. The Riemann invariants can be calculated from the measured microphone signals by solving Eq. (20), provided that at least two microphones were used. The solution in the least-squares sense is given by

$$\begin{bmatrix} \hat{f} \\ \hat{g} \end{bmatrix} = Z^{\dagger} \begin{bmatrix} \hat{p}_1 \\ \vdots \\ \hat{p}_N \end{bmatrix} \tag{21}$$

The acoustic velocity at the reference position is then given by $\hat{u}(x=0)=\hat{f}-\hat{g}$. Using the matrix notation, this can conveniently be expressed as

$$\begin{bmatrix} \hat{p}^A & \hat{p}^B \\ \hat{u}^A & \hat{u}^B \end{bmatrix} = \begin{bmatrix} 1 & 1 \\ 1 & -1 \end{bmatrix} Z^{\dagger} \begin{bmatrix} \hat{p}_1^A & \hat{p}_1^B \\ \vdots & \vdots \\ \hat{p}_N^A & \hat{p}_N^B \end{bmatrix} \tag{22}$$

Applying the operation of Eq. (22) to both the microphones upstream and downstream of the element yields the matrix with acoustic pressures and velocities required to solve Eq. (19) for T.

4.1 Flame Transfer Matrix. In order to measure a transfer matrix, arrays of microphones have to be placed at both sides of the element. Since a flame is always stabilized by some kind of flame holder (the "burner"), it is not possible to measure a flame transfer matrix directly. However, the transfer matrix of the combined burner and flame element (**T**) can be measured, along with the transfer matrix of the burner (**B**) only (in the absence of combustion but with flow). The desired flame transfer function (**F**) can then easily be obtained from

$$\mathbf{F} = \mathbf{T}\mathbf{B}^{-1} \tag{23}$$

The underlying assumption is that the transfer matrix (**B**) does not change due to the combustion process.

5 Results

Prior to the transfer function measurement experiments, a calibration experiment was performed by operating the test facility at three adiabatic flame temperatures and four mixture mass flow settings. The time traces of the chemiluminesence data were recorded. In order to get an estimate of the mean intensities of the signals, the median value of the time traces was evaluated. These values are plotted in Fig. 3 for the signal of CW307. The values of k and α in Eq. (2) were solved for in least-squares sense by linear regression of the measured data. Linear regression could be used because $\ln(I/m)=\ln(k)+\alpha\ln(T)$ is linear in the parameters $\ln(k)$ and α. The results of this curve fit are shown in Fig. 4 as well. Note that during the temperature variation experiment, the velocity was not held exactly constant. This explains why the fitted trend line does not coincide with the fitted data points. A similar

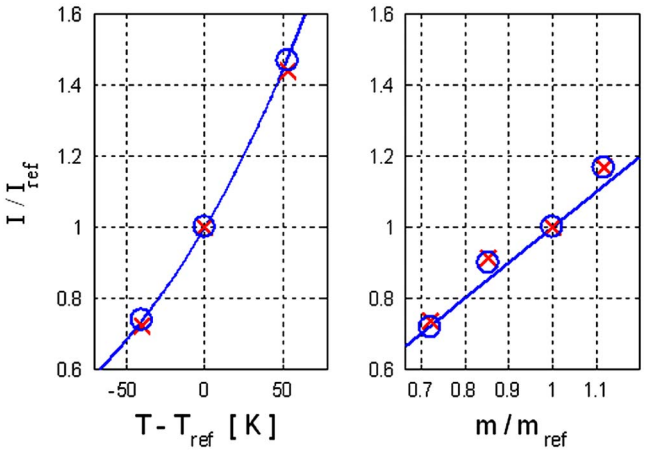

Fig. 3 Normalized mean chemiluminescence intensity as a function of adiabatic flame temperature and mixture mass flow. Crosses: measured data; circles: data fit using Eq. (2); solid line: trend line of Eq. (2)

fit was performed for the other chemiluminesence signals. Remarkably, the curves were very similar with only about 10% difference in the value of the exponent α. The values of α for all five signals are shown in Table 1 together with the fitting statistics. The relative error E represents an average value of the normalized residuals of the fit $E=1/N\Sigma_n|I_n-\tilde{I}_n|/In$. The value of R^2 is a measure for the explained variation of the data. It is defined as one minus the variance of the residuals divided by the variance of the data. It was tabulated together with the values obtained for α in Table 1. Considering that only two parameters were fitted to six data points, the fit is remarkably good. A transfer function experiment was carried out by applying a sequence of pure tone excitations to the loudspeakers. Excitation was applied upstream and downstream consecutively. The response of the nine microphones and the five chemiluminescence signals was recorded, and the Fourier coefficients at the forcing frequency were evaluated. The multimicrophone method (Eq. (22)) was used to obtain the acoustic velocities and pressures at the burner exit plane. First, a test without combustion was done in order to obtain the burner transfer matrix **B** using Eq. (19). A similar test with combustion was carried out. From the measured acoustic signals, the heat release

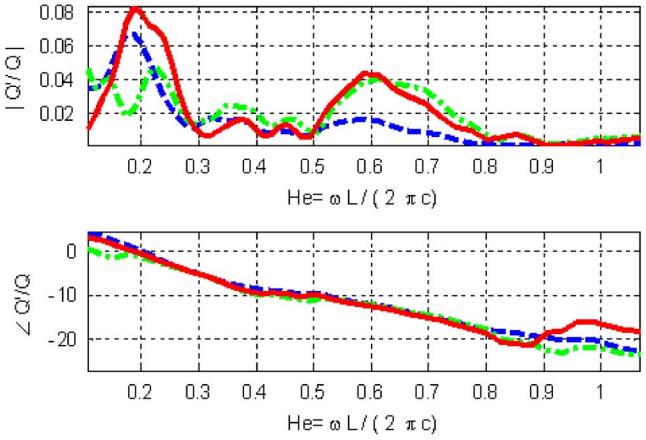

Fig. 4 Comparison of heat release obtained from acoustic data (dashed) with heat release obtained from optical data according to Eqs. (11) and (3) (solid) and the relative OH* intensity fluctuations (dash-dotted)

Table 1 Results of curve fitting the data with Eq. (2); values of α, the relative error E in %, and the goodness of fit R^2 in %

Filter	No filter	F_1	F_2	F_3	F_4
α/α_r	1	1.13	1.05	0.93	0.91
E	1.2	1.3	1.3	1.1	1.5
R^2	99.6	99.6	99.6	99.6	99.4

fluctuations were calculated by making use of the Rankine–Hugeniot relation (Eq. (15)) and the previously measured burner transfer matrix

$$\frac{\hat{Q}}{\bar{Q}} = \frac{\hat{u}_2 - B_{12}\hat{p}_0 - B_{22}\hat{u}_0}{\left(\frac{T_2}{T_1} - 1\right)\bar{u}_1} \tag{24}$$

The relative heat release fluctuations (i.e., the Fourier coefficients of the heat release signal divided by the mean heat release) were also calculated from the optical signals by making use of Eqs. (3) and (11). A comparison between the results of the purely optical method and the purely acoustical method for obtaining the heat release is shown in Fig. 4. The comparison shows a very good agreement of the phase while the agreement of the absolute value is reasonable for lower frequencies, but shows stronger deviations for higher frequencies. In some literature references, the relative intensity fluctuations are interpreted as relative heat release fluctuations. For comparison, this quantity was also plotted in Fig. 4. Although the phase matches reasonably, the absolute values do not even capture the trends. As will be shown later, the main component of the heat release fluctuations in this case is due to mass flux fluctuations. Note that if the interaction would take place via equivalence ratio fluctuations, then the relative intensity fluctuations would be an order of magnitude larger than the values recorded here. Clearly, the method proposed in this paper is not biased by prior assumptions on the nature of the interaction mechanism.

From the acoustic data available, the flame transfer matrix **F** is calculated using Eqs. (19) and (23). The result is plotted in Fig. 5 for the F_{12} and F_{22} elements. In the same figure, the flame transfer matrix elements obtained from the optical data are plotted (using Eq. (16)). Although the match is not perfect, the comparison is reasonable both quantitatively and qualitatively. Note that the F_{12} element is considerably smaller than the F_{22} element, which means that the influence of velocity fluctuations on the transfer function is more important than the influence of pressure fluctuations. However, the influence of pressure fluctuations on this burner is significant and should not be neglected. In order to investigate the nature of this transfer matrix, the transfer matrix C is analyzed. It was obtained from Eqs. (11) and (14) and shows how the mass flux fluctuations through the flame (i.e., flame surface or flame velocity fluctuations) and fuel mass fraction fluctuations depend on the acoustic pressure and velocity. The matrix elements are plotted in Fig. 6. This figure shows that the C_{12} element (which relates mass flux to velocity) is most dominant. The C_{22} element has a considerable magnitude as well, which means that fuel mass fraction fluctuations are caused by velocity fluctuations. This is a well known mechanism: If the injected mass flow of fuel is fairly constant, then a modulation of the velocity in the burner will cause equivalence ratio fluctuations at the injection location. This mechanism is explained in more detail in Refs. [6,7]. These concentration waves are convected with mean flow from the injector to the flame. Fuel mass fraction fluctuations caused by pressure fluctuations (C_{21}) are significantly smaller but not negligible. The physical explanation is that the fuel system is not entirely stiff, which means that pressure fluctuations cause a modulation of the fuel supplied by the injection holes. The C_{11} element describes the influence of the pressure fluctuations on the flame speed or area. For natural gas flames, the flame area and speed can be considered independent of the pressure. So, this term is indeed expected to be small. However, flame speed depends on the equivalence ratio and, as mentioned before, equivalence ratio fluctuations can be caused by pressure fluctuations.

As a check of consistency of the method, it is interesting to analyze the values of the C_{12} and C_{22} elements for frequencies approaching zero. For quasisteady changes of the velocity (i.e., approaching zero Hz), the relative mass flux through the flame front should be equal to the relative velocity in front of the flame. Hence, the C_{21} element should approach a value of +1 for zero frequency. Similarly, a quasisteady increase in velocity in the burner at constant mass flow of fuel results in a proportional de-

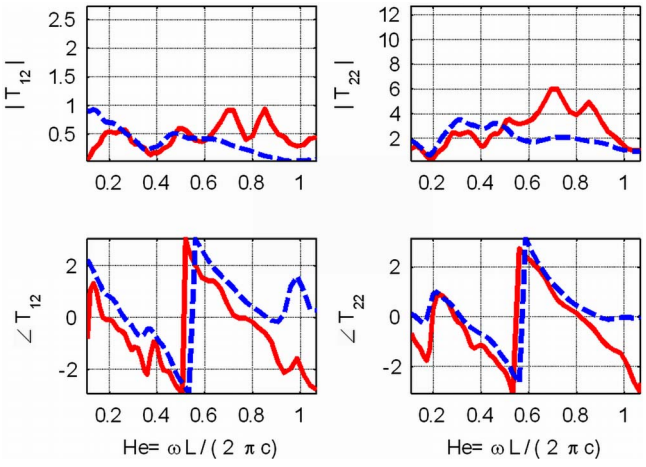

Fig. 5 Comparison of transfer matrix elements F_{12} and F_{22} obtained from acoustic data (dotted) using equation Eqs. (19) and (23) and obtained from optical data (solid) using Eqs. (11), (14), and (16)

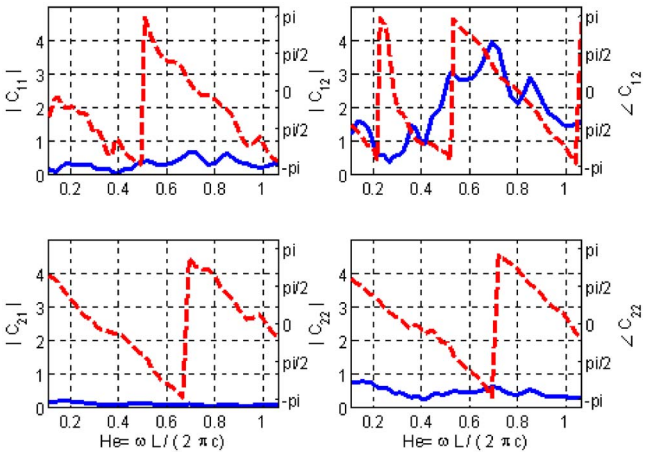

Fig. 6 Absolute values (solid) and phase (dashed) of the matrix elements of C

crease in the mass fraction of fuel. Hence C_{22} should be -1 at 0 Hz. Note that the lowest frequency measured was a Helmholtz number of He=0.1; however, one can reasonably estimate from Fig. 6 that toward zero frequency, both elements have an absolute value of about 1, while the phase of C_{12} assumes a value of close to zero and the phase of C_{22} a value of about π, which demonstrates that at least the very basic physical conservation laws are correctly represented by this matrix.

6 Discussion

Both the newly developed optical method for measuring transfer matrices and the acoustic approach yield similar results. As mentioned before, the two methods have a significant difference in the absolute values for the high frequencies. This difference can be due to uncertainties in both the optical and the acoustic method. The main possible sources of uncertainty of the optical method are as follows: (1) The optical arrangement does not have a spatially uniform efficiency (i.e., light of equal intensity emitted from different regions of the combustion chamber is measured with a different intensity). Because of this, an intensity fluctuation due to periodic flame motion could be recorded, although this does not represent fluctuating heat release. (2) The inversion operation in Eq. (11) may cause strong sensitivity to measurement uncertainty if J is badly conditioned (i.e., if the rows of matrix J are linearly dependent). Indeed, the values of α (Table 1) do not differ strongly. However, an error analysis shows that the discrepancy cannot be explained by this. (3) It was assumed that the flame is spatially homogeneous. If this is not the case (i.e., there are hot spots in the flame), then Eq. (2) will no longer be valid for the integrated light intensity. However, because measured levels of NO_x emissions were low during the experiment, it is likely that the temperature distribution was homogeneous. (4) It is assumed that the intensity signals are proportional to the fluctuating heat release components. In case a quasisteady component contributes to the signal (e.g., black body radiation of the liner), this would bias the calibration process. It is, however, not expected that to be the case here because the liner temperature was cold enough to avoid components in the UV bands. (5) It is assumed that the time scale of the chemical reaction is much smaller than acoustic or convective time scales. If this is not true, then the matrix J would not be constant but frequency dependent. For the range of frequencies considered here, we may consider this assumption to be valid. (6) Linearization is applied, which implies that the fluctuation amplitudes are assumed small enough.

The main sources of uncertainty in the acoustically measured transfer function are as follows: (1) *Speed of sound downstream of the combustion zone*. Although the adiabatic flame temperature can be obtained with reasonable accuracy (from the measured mass flow, temperature, and composition of the mixture), the heat flux through the cooled combustion chamber liners is more difficult to estimate. A resulting error in the speed of sound may cause problems when using the multimicrophone method. The introduced error can be very large in the case of resonant behavior. The relative error is of order $\frac{1}{2}Z$ He times the normalized error in the temperature, where Z is the specific impedance of the test rig. Since the test rig is nearly anechoic $Z \approx 1$ and $\mathrm{He} \approx 1$, then even an error in the temperature as large as 100 K will not cause an error larger than 3% in worst case conditions. (2) The inversion of the burner transfer matrix in Eq. (23) introduces an uncertainty, which is more difficult to quantify. It was assumed that the burner transfer matrix measured in the reactive case is the same as in the nonreactive case, which is difficult to verify.

The determination of the matrix C allows for an assessment of the underlying physical mechanisms of the thermoacoustic interaction processes. It directly relates the contribution of the fuel system interaction, equivalence ratio fluctuations, and flame front dynamics on the heat release. For the test burner under investigation, the most important coupling mechanism was found to be the flame front dynamics (mass flux fluctuations). However, as various investigations have shown, this is not always the case: Depending on the type of burner, either fuel system interactions or equivalence ratio fluctuations may become dominant.

7 Conclusions

A novel method for the experimental determination of flame transfer matrices was presented. The proposed method makes use of multiple chemiluminesence signals. The method has the advantage since it directly reveals the nature of the interaction mechanism because it allows for the identification of the contribution of equivalence ratio fluctuations and flame front dynamics in an intermediate step. A proof of concept is given by comparing this method with a purely acoustic method for measuring flame transfer functions. The quantitative agreement between the two methods is reasonable. Possible causes for the difference are discussed. The method was applied to a full-scale prototype gas turbine burner and quantified the underlying interaction mechanisms: fuel system interaction, equivalence ratio fluctuations, and flame front dynamics. Due to the stiff fuel system and distributed fuel injection, the first two interaction mechanisms were found to be less pronounced, which made the flame front dynamics the dominant interaction mechanism.

Acknowledgment

This work was conducted in the framework of AG Turbo/COOREFF-T. The authors would like to acknowledge Brian Cox for his assistance in the experiments, Daniel Guyot (TU Berlin) for his interesting discussions on the feasibility of the proposed method, and Peter Flohr for his support of this work.

Nomenclature

A_f = flame area
H_f = chemical enthalpy
He = Helmholtz number, $\mathrm{He}=\omega L/(2\pi c)$
I = chemiluminesence intensity
Q = heat release rate
S_f = flame speed
T = temperature
c = speed of sound
m = mass flux through flame surface
p = pressure
u = velocity
y = fuel mass fraction
γ = ratio of specific heats
ρ = density
ω = angular frequency
$\bar{x}$ = steady component of x
$x'(t)$ = unsteady component of x, $x'(t) \equiv x(t) - \bar{x}$
$\hat{x}(\omega)$ = Fourier coefficient of $x'(t)$

References

[1] Cremer, L., 1971, "The Treatment of Fans as Black Boxes," J. Sound Vib., **16**(1), pp. 1–15.
[2] Bodén, H., and Åbom, M., 1986, "Influence of Errors on the Two-Microphone Method for Measuring Acoustic Properties in Ducts," J. Acoust. Soc. Am., **79**(2), pp. 541–549.
[3] Paschereit, C. O., Schuermans, B., Polifke, W., and Mattson, O., 2002, "Measurement of Transfer Matrices and Source Terms of Premixed Flames," ASME J. Eng. Gas Turbines Power, **124**(2), pp. 239–247.
[4] Paschereit, C., Schuermans, B., Polifke, W., and Mattson, O., 1999,"Measurement of Transfer Matrices and Source Terms of Premixed Flames," ASME Paper No. 99-GT-0133.
[5] Schuermans, B., 2003, "Modeling and Control of Thermoacoustic Instabilities," Ph.D. thesis, EPFL Lausanne, Switzerland, http://library.epfl.ch/theses/?nr=2800.
[6] Schuermans, B., Polifke, W., and Paschereit, C., 1999, "Modeling Transfer Matrices of Premixed Flames and Comparison With Experimental Results," ASME Paper No. 1999-GT-0132.
[7] Schuermans, B., Bellucci, B., Guethe, F., and Meili, F., 2003 "A Detailed Analysis of Thermoacoustic Interaction Mechanisms in a Turbulent Premixed Flame," ASME Paper No. GT-2004-53831.

[8] Bellucci, V., Schuermans, B., Nowak, D., Flohr, P., and Paschereit, O., 2003, "Thermoacoustic Modeling of a Gas Turbine Combustor Equipped With Acoustic Dampers," ASME Paper No. GT-2004-53977.
[9] Langhorne, P., 1988, "Reheat Buzz: An Acoustically Coupled Combustion Instability. Part 1. Experiment," J. Fluid Mech., **193**, pp. 417–443.
[10] Poinsot, T. J., Trouve, A. C., Veynante, D. P., Claudel, S. M., and Esposito, E. J., 1987, "Vortex-Driven Acoustically Coupled Combustion Instabilities," J. Fluid Mech., **177**, pp. 265–292.
[11] Auer, M. P., Hirsch, T., and Sattelmayer, T., 2006, "Influence of Air and Fuel Mass Flow Fluctuations in a Premix Swirl Burner on Flame Dynamics," ASME Paper No. GT-2006-90127.
[12] Haber, L., Vandsburger, U., Saunders, W. R., and Khanna, V., 2006, "An Examination of the Relationship between Chemiluminescent Light Emissions and Heat Release Rate under Non-Adiabatic Conditions," ASME Paper No. GT-2000-GT-0121.
[13] Higgins, B., McQuay, M., Lacas, F., Rolon, J., Darabiha, N., and Candel, S., 2001, "Systematic Measurements of OH Chemiluminescence for Fuel-lean Highpressure, Premixed, Laminar Flames," Fuel, **80**, pp. 67–74.
[14] Higgins, B., McQuay, M., Lacas, F., and Candel, S., 2001, "An Experimental Study of Pressure and Strain Rate on CH Chemiluminescence on Premixed Fuellean Methane/Air Flames," Fuel, **80**, pp. 1583–1591.
[15] Hardalupas, Y., and Orain, M., 2004 "Local Measurements of the Time-Dependent Heat Release Rate and Equivalence Ratio Using Chemiluminescent Emission From a Flame," Combust. Flame, **139**, pp. 188–207.
[16] Ayoola, B. O., Balachandran, R., Frank, J. H., Mastorakos, E., and Kaminski, C. F., 2006, "Spatially Resolved Heat Release Rate Measurements in Turbulent Premixed Flames," Combust. Flame, **144**, pp. 1–16.
[17] Zajadatz, M., Bernero, S., Lachner, R., and Motz, C., 2007, "Development and Design of Alstom's Staged Fuel Gas Injection EV Burner For NO_x Reduction," ASME Paper No. GT 2007–27730.
[18] Kojima, J., Ikeda, Y., and Nakajima, T., 2000, "Detailed Distributions of OH^*, CH^* and C_2^* Chemiluminescence in the Reaction Zone of Laminar Methane/Air Premixed Flames," 36th AIAA/ASME/SAE/ASEE Joint Propulsion Conference and Exhibit, Paper No. AIAA-3394.
[19] Nori, V., and Seitzman, J., 2007, "Detailed distributions of OH^*, CH^* and C_2^* Chemiluminescence in the Reaction Zone of Laminar Methane/Air Premixed Flames," 45th Aerospace Sciences Meeting, Reno, NV, Jan. 8–11, Paper No. AIAA-2007-0466.